Available online at www.sciencedirect.com
ScienceDirect
Journal of Marine Systems 68 (2007) 215–236
JOURNAL OF MARINE SYSTEMS
www.elsevier.com/locate/jmarsys

A study of crab larvae dispersal on the Western Iberian Shelf: Physical processes

Alvaro Peliz [a,*], Patrick Marchesiello [b], Jesus Dubert [a], Martinho Marta-Almeida [a], Claude Roy [d], Henrique Queiroga [c]

[a] Departamento de Física (CESAM), Universidade de Aveiro, 3810-193 Aveiro, Portugal
[b] Institut de Recherche pour le Développement, BPA5, Noumea, New Caledonia
[c] Departamento de Biologia (CESAM), 3810-193 Aveiro, Universidade de Aveiro, Portugal
[d] Centre IRD de Bretagne, BP70, 29280 Plouzané, France

Received 22 June 2005; received in revised form 25 May 2006; accepted 14 November 2006
Available online 19 January 2007

Abstract

A high resolution nested model of the Western Iberia shelf is developed and compared with field observations. We use an embedded particle tracking submodel that includes advection, diffusion, and diel vertical migration to simulate crab larvae dispersal. A set of experiments with varying oceanographic conditions and Lagrangian model parameters is analysed. It is found that major dispersal patterns that were observed in nature are reproduced in the model. The floats drift within meridionally elongated patches parallel to the coast usually inshore of the 100 m isobath. This distribution is controlled by local wind-driven circulation, buoyancy input from adjacent rivers, local topography, and vertical diel movements. River plumes are critical factors for retention patterns as they influence the near surface stratification, surface Ekman layer and innershelf processes. Weakly stratified coastal waters associated with low river run-off generate an enlarged innershelf whose dynamics tend to trap the floats and force them to drift along-wind. We find that the response to downwelling-favourable winds is always more dramatic than upwelling-favourable ones and this asymmetry results in a net Lagrangian transport directed poleward. Analyses of float distributions show that a large part of the floats (~50%) is actually retained in the shelf zone near the emission points. A dispersal distance (L_d) of about 60 km is estimated which is mostly representative of along-shore dispersion. Some consequences of our results to local population dynamics are finally discussed.

Keywords: Western Iberia; Larval dispersal; Dispersal distance; Crab larvae

1. Introduction

The Western Iberia Shelf (Fig. 1) is a seasonal upwelling system where persistent northerlies (upwelling-favourable) are observed in summer (June to September) with the development of typical upwelling phenomena like coastal jets and long filaments (e.g., Haynes et al., 1993; Peliz et al., 2002; Álvarez-Salgado et al., 2003). It is, however, during the non-upwelling season (late winter-spring) that a large amount of meroplankton species are observed over the shelf (e.g., Santos et al., 2004). During this season, the slope and outer shelf are under the influence of the Iberian Poleward Current (IPC; e.g., Peliz

* Corresponding author.
E-mail address: apeliz@fis.ua.pt (A. Peliz).

0924-7963/$ - see front matter © 2006 Elsevier B.V. All rights reserved.
doi:10.1016/j.jmarsys.2006.11.007

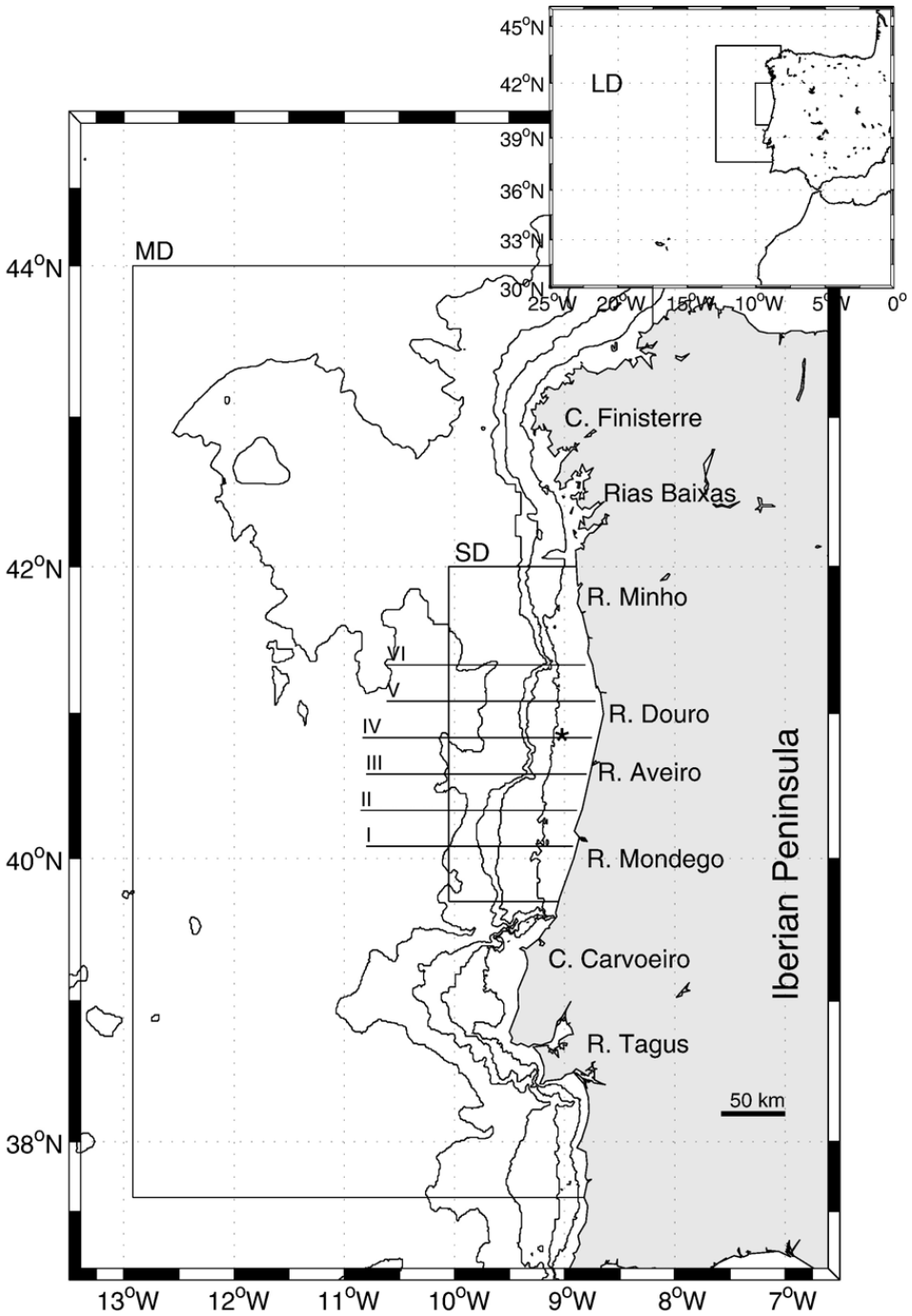

Fig. 1. Map of the study zone and model domains. The large model domain (LD) is represented in the inset. Boxes show the medium domain (MD) and the small domain (SD). The 3000, 1000, 200 and 100 m isobaths are represented. Cross-shelf sections of the 1991 spring cruise are shown (lines across the shelf numbered I–VI). The main geographical sites referred in the text are indicated. A star indicates the mooring position (~9°W, 41°N).

et al., 2003, 2005) which is a meandering and eddy shedding feature. On the other hand, a large portion of land runoff from Iberian Peninsula is directed to the shelf zone between Tagus and Rias Baixas (see Fig. 1) generating a surface low salinity layer termed the Western Iberia Buoyant Plume (WIBP; e.g., Peliz et al., 2002; Santos et al., 2004). The joint effect of both these features (WIBP and IPC) together with alternating downwelling and upwelling episodes, creates extremely variable circulation patterns at short time scales, from a few days to weeks, in which the plankton disperse. The influence of these flow structures upon the dispersion patterns is very poorly studied. Santos et al. (2004) present a simplified modelling study and draw the attention to the influence of mesoscale features other than the wind-driven currents in the dispersal of sardine larvae. Marta-Almeida et al.

(2006) show that the interplay between the larvae Diel Vertical Migration (DVM) and cross-shelf circulation induced by Ekman dynamics can produce complex dispersion pathways. In some cases, upwelling-favourable events may contribute to larvae retention near the coast.

The main objective of this work is to study the role of different physical processes on the dispersal patterns of crab larvae, and to estimate the dispersal length (e.g. Largier, 2003; Shanks, 2003) and transport. The final goal is then to understand how these processes influence local population dynamics. We analyse results from a numerical study conceptualised and validated using a plankton and hydrography survey conducted off Western Iberia in the spring of 1991. For the larvae dispersal experiments, a single target species is used (*Carcinus maenas*).

This crab species is interesting from the oceanographic point of view due to its planktonic larval phase. The sites and periods of larvae emission to the shelf are relatively well known. The larvae are released to the shelf from coastal points with resident adult populations (major estuarine systems). After the planktontrophic larval phase that occurs over the shelf during a few weeks, larvae have to return to the estuaries for successful settlement and metamorphosis. Hatching occurs in the lower part of the estuaries during nighttime ebbing tides (Queiroga et al., 1994). Newly hatched larvae migrate vertically in synchrony with the tidal cycle, attaining the highest position in the water column during ebb (Queiroga et al., 1997). This migration ensures that most of the larvae are exported to the sea within one tidal cycle. Larval development proceeds through four zoeal stages and one megalopa (Rice and Ingle, 1975), which is the stage that reinvades the estuaries. Larval development of the megalopa spans from 35 to 50 days (Dawirs, 1985; Nagaraj, 1993) at the temperatures normally found in Portuguese coastal waters during the species reproductive season from January to July. Reinvasion of the estuaries takes place during night flood tides (Queiroga, 1998) by selective tidal stream transport.

Larvae of most crabs and other decapod crustaceans undergo extensive DVM in shelf waters, ascending to the surface layer during the night (Queiroga and Blanton, 2005). Since the Lagrangian model is tested with various DVM scenarios, the results can be more generally applied to other meroplanktonic species.

The paper is organised as follows: Data and methods (Section 2) contains a summarised description of the field data used in the study followed by a detailed description of the oceanic and Lagrangian model. The ocean model results are compared with observations in Section 3.1. The remaining part of the results section is dedicated to the analysis of the Lagrangian model, dispersal length statistics, transport statistics, and varying oceanographic conditions. The results are discussed in Section 4 and a summary of conclusions is presented at the end.

2. Data, models and methods

2.1. The April 1991 survey

Hydrology and currents off Western Iberia (Fig. 1) were observed in Spring 1991 in the frame of the Eastern Boundary Currents program of the World Ocean Circulation Experiment (WOCE II; Hagen, 1994). An almost synoptic shelf-slope-scale distribution of plankton larvae (with vertical stratification) timely with CTD and currents was obtained. The survey comprised a set of cross-shore sections conducted between the 2nd and 10th of April (denoted by I–VI in Fig. 1). Details on instrument and data quality verification are provided in Hagen (1994). A currentmeter mooring was deployed during the survey with records starting from March 19 (14:00 UTC) and lasting until April 13 1991 (10:00 UTC) at the position 40° 47.4′N, 9° 06.2′W (the mooring position is indicated with a star in Fig. 1). The overall water depth was 105 m and three recording current meters (Aanderaa RCM-4) were deployed for 23 days at 40, 71, and 98 m, with a constant sampling interval of 10 min. The description of the currentmeter data is presented in Kline (2000). Unfortunately, the original current records were not available for the present research. In order to recover the currentmeter information, subinertial data was digitalised from report plots. Table 1 presents the statistics of the original data (from the reports and from the digitalised values).

The plankton samples were collected with a Multiple Opening Closing Net (MCN) which allowed a vertical discretisation in 30 m wide strata. No *C. maenas* larvae

Table 1
Currentmeter data statistics at 40 m[in cm/s]: i) Statistics based on original data reported in Kline (2000); ii) Statistics based on digitalised values from original cruise reports data plots; iii) Statistics based on model results at 37 m depth

	$\bar{u}$	Max(u)	Min(u)	$\sigma(u)$	$\bar{v}$	Max(v)	Min(v)	$\sigma(v)$
i	1.14	8.38	−6.92	2.85	−1.6	14.25	−24.5	9.79
ii	0.94	8.17	−7.37	2.94	−0.9	13.92	−24.8	8.24
iii	−0.47	3.85	−5.74	1.94	−1.36	4.74	−19.13	5.66

All data correspond to subinertial currents (filtered with a 41 hour window) for the period between March 19 and April 13.

were collected below 90 m. More than 90% of the first and second larval stages were concentrated above 30 m, but older stages tended to move deeper and equally distributed between the 0–30 m and 30–60 m strata. A detailed analysis of plankton data is presented in Queiroga (1996).

Winds and air-sea fluxes (daily averages) used in this work were taken from the National Centre for Environment Prediction (NCEP) reanalysis program. Winds for 41°N, 9° 35′W west of Portugal are shown in Fig. 3.

2.2. The ocean model

The ocean simulations were performed using the Regional Oceanic Modelling System (ROMS) described in Shchepetkin and McWilliams (2003, 2005). ROMS is a 3D free-surface sigma-coordinate split-explicit primitive equation model (with Boussinesq and hydrostatic approximations). The finite-difference discretisation algorithms are orientated toward nonoscillatory high-order schemes, thus improving the effective resolution of the model. In particular, a third-order upstream-biased advection scheme with implicit lateral diffusivity allows the generation of steep gradients, while a new pressure gradient algorithms ensures low levels of sigma-related errors. A 3rd order accurate corrector leapfrog/Adams–Moulton time step algorithm is used which allows a substantial increase of time step as well as good dispersive properties for the advection equation. The open boundary conditions are for the baroclinic mode a combination of outward radiation and flow-adaptive nudging toward prescribed external conditions, and for the barotropic mode a Flather-type condition to ensure well-posed tidal forcing (Marchesiello et al., 2001). Explicit lateral viscosity is null everywhere, except along sponge layers near open boundaries where maximum horizontal viscosity values are A_h $m^2/s=600$. Vertical mixing processes are parameterised with the non-local K-profile boundary layer scheme (Large et al., 1994) implemented for both surface and bottom boundary layers. The vertical diffusion terms are treated with a semi-implicit, Crank–Nicholson scheme to avoid time step restrictions due to large vertical mixing rates in the boundary layers and in the interior when static stability needs to be restored. A quadratic bottom drag coefficient is held constant over the entire domain to a value of $1.0.10^{-3}$.

Our strategy for managing the large range of scales involved in this study is a multi-level approach based on the AGRIF package. This is an online (synchronous) nesting procedure which allows a rapid setup of a series of embedded domains with increasing resolution (Penven et al., 2006). The model grids, forcing, initial and boundary conditions are built using the ROMSTOOLS package (Penven, 2003). The model configuration is for the midlatitude Eastern North Atlantic centred on the Iberian Peninsula (see Fig. 1). It includes three overlapping domains with different spatial resolutions (~16 km for the larger domain, LD; ~6 km for mesoscale grid, MD, and ~2 km for the smaller domain, SD). Vertical resolution is the same in the 3 domains. 30 sigma levels are used with sigma resolution increasing near the surface ($\theta s=7$ and $\theta_b=0$; e.g., Haidvogel and Beckman, 1999). Even in deep ocean areas, the surface Ekman layer is resolved and the spacing between the surface sigma levels is less than a few meters.

The experiment has been developed in 3 different stages. The first stage entails the spin-up of the large domain during three years to obtain an equilibrium solution (convergence of eddy kinetic energy to stationary mean value; e.g., Marchesiello et al., 2003). For this stage Levitus et al. (1994a,b) temperature and salinity data, and Comprehensive Ocean-Atmosphere Data Set (COADS; da Silva et al., 1994) were used to obtain initialisation and climatological fields for temperature, salinity, sea surface elevation, heat, mass and momentum surface fluxes and mean geostrophic currents. The second phase concerns the spin-up of the mesoscale domain with (6 km resolution) during a 3 month period to achieve a typical winter situation. Finally the third stage corresponds to the target simulation with all three domains to approximate spring 1991 cruise conditions. For this experiment the atmospheric forcing data were obtained from daily averaged NCEP reanalysis data which includes: momentum, surface heat fluxes, and solar shortwave radiation.

In this final stage, tidal elevation along the boundaries was included (the main contribution is given by M_2 and S_2 constituents (e.g., Marta-Almeida and Dubert, 2006). Point sources of mass, to simulate the river flow were introduced. Due to the lack of data regarding river runoff for the study period, the outflow was kept fixed at the following climatological values: Tagus, Minho, and Mondego — 500 m^3/s and Douro 800 m^3/s (see Fig. 1). Salinity of the outflow was fixed to 5 and temperature to 15.0 °C.

Since the Lagrangian experiments were conducted online, these final stage was repeated for each of the float experiments.

2.3. The Lagrangian model

A Lagrangian submodel (floats for brevity) presented in Capet et al. (2004) is used to simulate the larvae

emission and dispersion. The floats use the 3D model velocity fields for advection with a fifth-order scheme based on Adams–Bashforth/Adams–Moulton predictor–corrector time step algorithm. AGRIF has been adapted to manage the communication of floats through the different model domains. Besides the advection with the model velocities, we have implemented for this study additional components to the floats submodel, so that the float velocity u_f is calculated using:

$$u_f(x,y,z) = U_a(x,y,z) + u_r(x,y) + w_d(z) + w_r(z) \quad (1)$$

where U_a is the model 3D velocity vector, u_r is a random component introduced to the horizontal velocity vector using:

$$u_r = \delta\sqrt{2K_h/\Delta t} \quad (2)$$

where δ is a real uniform random number ($\delta \in [-1,1]$, and K_h is the imposed explicit Lagrangian horizontal diffusion of the form:

$$K_h = \varepsilon^{1/3} l^{4/3} \quad (3)$$

where l is the unresolved subgridscale (here taken as the cell size) and $\epsilon = 10^{-9}$ m^2/s^3, is the turbulent dissipation rate (e.g., Monin and Ozmidov, 1981).

Attempting to simulate the diel migration of larvae, a deterministic vertical movement is imposed:

$$w_d = \begin{cases} -30[\text{m/h}] & \text{if } 4<t_h<6 \\ 30[\text{m/h}] & \text{if } 22<t_h<24 \\ 0[\text{m/h}] & \text{otherwise} \end{cases} \quad (4)$$

where t_h is time of the day in hours. Vertical migrations are allowed down to a depth $d = \min(\max_d, h)$ where h is the local depth and $\max_d$ is either a fixed value (50 m) in the case of Base experiment, or a value depending on the zoeal stage in the case of Base 2 experiment (Table 2).

Finally, w_r stands for vertical random fluctuation associated with unresolved vertical turbulent fluxes. The formulation of w_r is based on the modelling study of Ross and Sharples (2004):

$$w_r = \delta\sqrt{2K/((1/3)\Delta t) + K_z} \quad (5)$$

where K is the vertical heat turbulent diffusivity taken from the KPP turbulent closer submodel, and K_z its vertical derivative. According to Ross and Sharples (2004) a correct implementation of Eq. (5) requires a time step constraint $\Delta t \ll \min(1/|K_{zz}|)$, where K_{zz} is the second vertical derivative of K. In order to respect this constraint, the Lagrangian model was implemented in a sub-time step relative to the main baroclinic model time step $\Delta t_{floats} = \Delta t/200 = 9$ s.

Table 2
Age and maximum depth of vertical migration for each zoeal stage

Zoea	I	II	III	IV	Megalopa
Age (days)	<9.5	<17.5	<26.1	<37.4	<37.4
Max depth (m)	28	28	31	37	40

Calculated using values from Queiroga (1996).

2.4. Lagrangian model sensitivity experiments

In order to test the Lagrangian model, a number of experiments were conducted using an idealised setup, i.e. a meridional periodic channel (northern hemisphere) configured as a shelf with the coast on its right side so that ($x=0$, $y=0$ is the southwestern corner point of the domain). The channel is 60 km wide in the cross-shelf direction (40 points, $\Delta x = 1.5$ km) and 120 km long in the along-shore direction (40 points, $\Delta y = 3$ km) The model bathymetry is kept constant at 150 m within 15 km of the offshore boundary and then ramps linearly to 5 m minimum depth at the coast. In the vertical, 30 levels are used with stretching factors: $\theta_s = 3$, $\theta_b = 0$. No slippery walls and linear bottom drag equal to $3 \cdot 10^{-4}$ m/s are imposed. No explicit horizontal diffusion or mixing are applied ($A_h = 0$). KPP is used for vertical mixing parameterisation. With the exception of one experiment, the salinity is constant (36.0) and the temperature has a 1 °C variation between surface and bottom ($T(z) = 14 - z/150$ °C). The only forcing of the system is the meridional (along-channel) wind stress $\tau_y = -0.05\sin(2\pi t_{days}/12)$ resulting in a 6 day period of upwelling followed by a 6 day downwelling in a total of 12 days. In one case, an initial band (from the surface to the bottom) of lower salinity (34.5) is introduced in the inner part of the shelf (15 km of the coast) to simulate the effect of river plumes. The floats are initiated along a zonal line (coastward of 100 m isobath) at 2 m depth. The float's initial y-position is near the northern bound of the domain ($y = 105$ km), since the first wind-stress pulse is upwelling-favourable and southward drift is expected. A summary of various sensitivity tests is presented in Table 3. The corresponding results are shown in Fig. 2.

In the case of the Base experiment (Fig. 2 a) the floats drift along isobaths with little offshore dispersion. The

Table 3
Summary and naming convention for the Lagrangian model sensitivity experiments

Name	Components	Description
Base	$U_a+u_r+w_d+w_r$	Experiment with all components
Nd	$U_a+u_r+w_r$	No migrations ($w_d=0$)
Nh	$U_a+w_d+w_r$	No horizontal diffusion ($u_r=0$)
NV	$U_a+u_r+w_d$	No vertical diffusion ($w_r=0$)
Base+riv	$U_a+u_r+w_d+w_r$	Base with river runoff

main result of the DVM is to integrate the velocity of the different layers in the float paths. A separation occurs between floats released in water depths above 50 m and those in the shallower part of the shelf (note the divergence of float paths near the 60 m isobath). The latter initially tends to migrate inshore since their daytime depth (associated with the DVM) is coincident with the inshore-flowing bottom Ekman layer. At the frictional innershelf where bottom and surface layers meet, this effect is not noticeable; the floats tend to migrate downwind along the topography, consistent with the analytical solution proposed by Estrade (2006). In deeper parts of the domain (>50 m), an offshore component of dispersion is observed.

The experiment with no DVM (Fig. 2b) produce float paths with the most significant cross-isobath dispersion. This is a consequence of the fact that the floats concentrate inside the surface Ekman layer (see float depth distribution for this experiment). Results for experiments with no horizontal diffusion (Fig. 2c) or

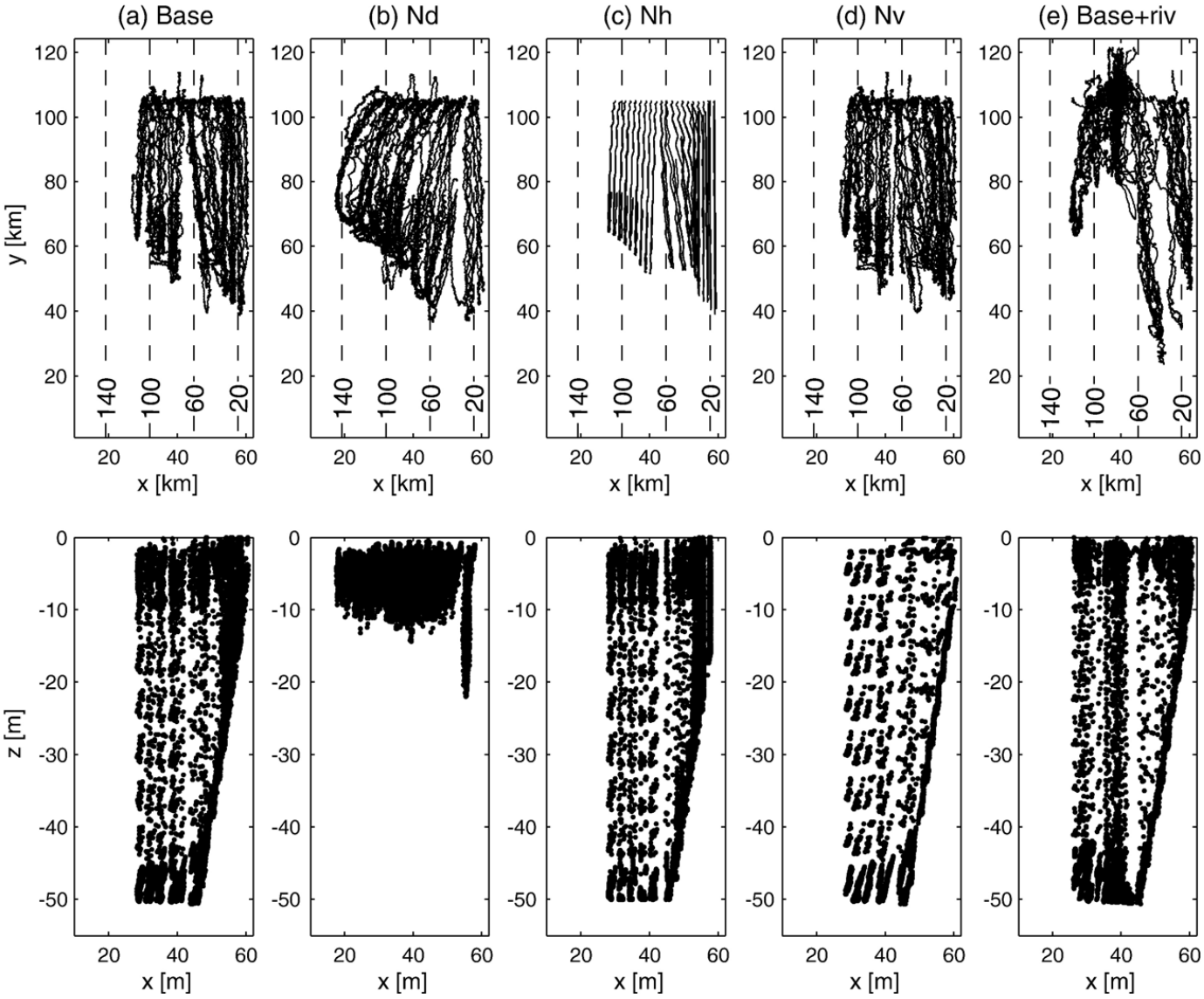

Fig. 2. Lagrangian model sensitivity experiments: a) Base, b) Nd, c) Nh, d) Nv, and e) Base+riv. Upper row shows the float paths in the horizontal plan (x, y) with model isobaths 140, 100, 60, 20 m. Lower row shows the float positions in the cross-shore/depth plan (x, z). For clarity of the plot only a few floats are shown in the vertical representation.

with no vertical diffusion (Fig. 2d) do not show substantial differences from the base experiment. This may be related to the absence in this experiment of significant vertical and horizontal shear in the ambient flow. The second most significant offshore dispersion (after the no-DVM case) is found for the river plume experiment (Fig. 2e). The associated stratification induces a thinner Ekman layer. Since diel migration forces floats to surface during nigh-time, the transport inside this thin Ekman layer will be larger.

There is still an additional effect associated with the nature of the vertical diffusion scheme. The first term in the right hand side of Eq. (5) stands for the random vertical fluctuations which will be shorter in regions of smaller K. The second term K_z is deterministic and forces floats to concentrate at the level of maximum K located in the surface and bottom boundary layers (SBL and BBL respectively). In the case of increased near surface stratification (induced by buoyant plumes), a thinner SBL is produced, and the maximum of K is found closer to the surface, forcing floats to oscillate around a shallower level. Since the stratification reduces K, the vertical particle excursions will be shorter. The final effect is float trapping (during night-time) in the surface Ekman layer. This effect emerges from the comparison between the different vertical float distributions of Fig. 2. The Base case (a) shows higher concentration of floats in the top 10 m. In the case with no vertical diffusion scheme (d), no clear float trapping is observed. Finally, in the river plumes experiment (e), float trapping occurs in a shallower layer (~5 m).

2.5. Lagrangian experimental set up in realistic simulations

From now on, the realistic configuration described in Section 2.2 is used to compare the Lagrangian model solution with observed larvae distributions. In this case, the floats are released at multiple times during the simulation period. Considering the limitations in the existing knowledge about larvae emission to the shelf (see Introduction) some assumptions had to be made: i) Emission of larvae occurs at ebb tides during 7 days centred at the peak of neap tides from 0 to 6 am (100 larvae per day at the beginning of the emission period and 300 at the peak). The central days of float emission are: February 10, February 24, March 10, March 24 and, April 6 (see Table 4). ii) Initial emission starts at February 10, since older larvae collected during the cruise should have been released to the shelf water not before the neap tide period centred on February 9. iii) Since the model does not resolve the estuary-shelf fluxes the larvae release is done randomly within a 4 km circle out of the estuaries of Mondego, Douro and Ria de Aveiro lagoon (see Fig. 1). iv) The experiments last until the end of the survey (April 10).

Table 4
Dates of float release in the Lagrangian model and float stages during the cruise period (calculation based on tidal and maturation data from Table 2)

Release day	February 10th	February 24th	March 10th	March 24th	April 6th
Stage	M	Z4 or M	Z3 or Z4	Z2	Z1

The table also provides an indication of most probable emission dates for each larval stage observed during the cruise (~April 6).

Table 5
Summary and naming convention for the float experiments

Name	Components	Description
Base	$U_a+u_r+w_d+w_r$	Experiment with all components
Base2	$U_a+u_r+w_d+w_r$	Base with $\max_d$ as function of age
Nd	$U_a+u_r+w_r$	No diel migrations ($w_d=0$)
Nh	$U_a+w_d+w_r$	No horizontal diffusion ($u_r=0$)
Nv	$U_a+u_r+w_d$	No vertical diffusion ($w_r=0$)
Nriv	$U_a+u_r+w_d+w_r$	Base with no river runoff
Nreduriv	$U_a+u_r+w_d+w_r$	Base with reduced river runoff
Base2000	$U_a+u_r+w_d+w_r$	Base experiment with 2000 forcing
Base2001	$U_a+u_r+w_d+w_r$	Base experiment with 2001 forcing

A total of 9 experiments are presented (summary in Table 5). The Base experiment uses the central ocean model experiment and all the float components. The next three variations concern only the Lagrangian model components. In Base 2 the vertical float migration is dependent on float age as described in Table 2. Nh stands for the experiment where no horizontal diffusion is added, and Nv for the one with no vertical migration. The other four experiments conserve the same Lagrangian set up as in the Base experiment but with variation in the oceanographic conditions: Nriv — no river runoff, and Base2000 and Base2001 the Base experiment but with atmospheric forcing for different years.

2.6. Metrics for model — observation comparison and analysis

Comparison between observed larvae concentrations and model floats is possible only in relative terms. No absolute values of larvae emission and mortality are known. On the other hand, measurements concern estimates of larvae density/area and not absolute concentrations. Dispersal distance (or length of dispersion — L_d) is not strongly dependent on absolute values

and can be estimated based on existing observations or model results. The model-observations comparison is conducted using metrics based on L_d. For the observations, $L_d = \Sigma_i(n_i d_i)/\Sigma_i n_i$ where i refers to the station number, n the number of individuals/m^2 and d the distance to the Ria de Aveiro (assumed to be the most significant emission point of larvae inside the observed zone Fig. 1). Using the same method, we have also calculated the mean and standard deviation of the zonal (l_x, s_x) and meridional (l_y, s_y) dispersion which approximately correspond to the cross-shore and along-shore components of dispersion.

The dispersal distance used here is a length scale representative of the mean distance where patches can be found away from their emission point regardless of direction, whereas s gives a measure of patch size and patch diffusion. In the case of Lagrangian experiments the calculation of dispersion metrics is straightforward: Since each float has a known position at the time of the survey, l, and s can be calculated using mean and standard deviation of float distance from emission point. For consistency with observations, we use only those floats that are within the limits of the survey area at the time of the survey (Fig. 1). The same emission point is used to calculate the distances (Ria de Aveiro).

3. Results

3.1. Shelf oceanography: observations and model results

A stick plot of NCEP winds (40.9°N 9.4°W) for the study period is presented in Fig. 3. Winds were generally weak and variable almost all the time. However, during the currentmeter record period (19 March to 13 April), a weak (rarely exceeding 5 m/s) but considerably persistent (about 20 days) upwelling event took place. Two peaks can be noticed: one centred around March 24 and the second around April 6 during the CTD survey.

Fig. 4 shows the observations (left column) and model (right column) near surface (10 m) distributions of salinity (upper row) and temperature (bottom row). Model and observation fields are displayed with the

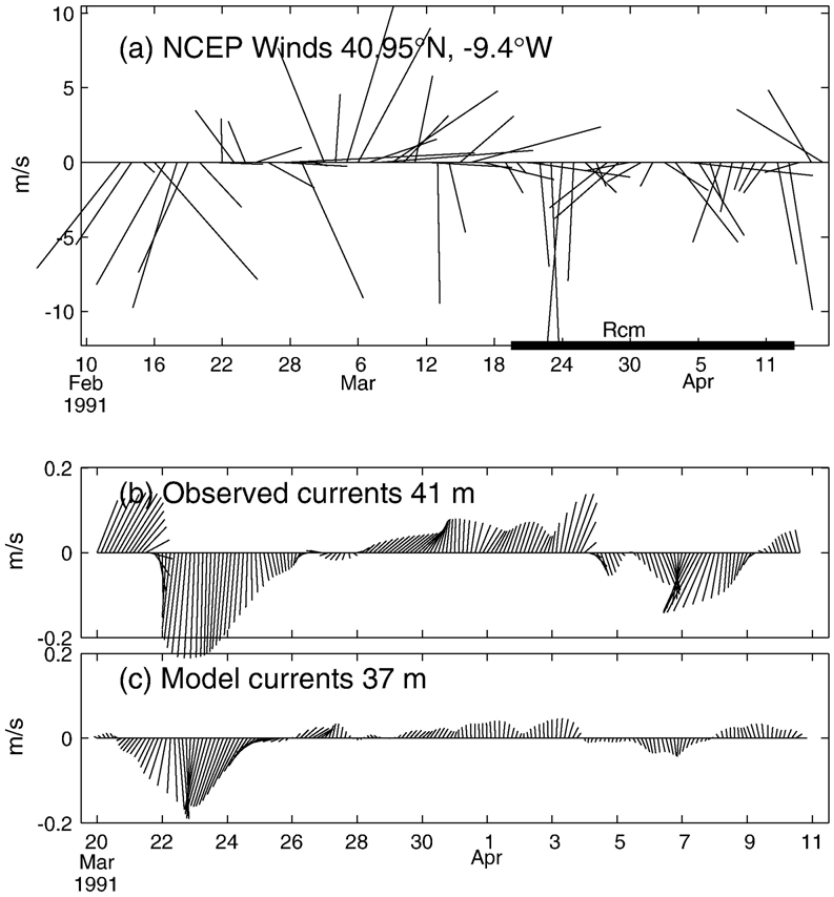

Fig. 3. Stick plots of NCEP winds and currents. a) NCEP reanalysis daily averaged winds at 40.9°N 9.4°W for the modelling period. A black line along time axis indicates the currentmeter record. b) Observed currents (subinertial) at 41 m depth at the mooring represented on the map in Fig. 1. c) Model current time series at 37 m for the same position.

same scaling and only the model-observations overlapping area is represented (we only show results from the small model domain presented in Fig. 1). Signatures of the dominant circulation patterns are apparent. Off the shelf the meridional gradients of temperature and salinity are associated with the Iberian Poleward Current (e.g., Peliz et al., 2005). Water is warmer and saltier in the south, mainly at deeper levels, i.e. away from the influence of surface buoyant plumes (not shown). Stronger gradients are found in the cross-shore direction and are associated with the Western Iberia Buoyant Plume. Cooler and significantly fresher waters are present all over the shelf. The cooling takes place near the surface due to contact heat loss to the colder air masses during northerlies (e.g., Santos et al., 2004).

The model (Fig. 4b, d) reproduces the major observational features, namely: the warmer/saltier waters at the slope and the fresher/cooler waters over the shelf. Model fields show a larger number of small scale structure when compared with observed fields due to the smoothing effect of the space and time sampling of the CTD survey. The elongated (filament-like) tongue evidenced by the 35.7 isohaline in the observed salinity field north of 41°N (Fig. 4d around 40.8°N) is advected off the shelf as the model WIBP interacts with slope current eddies after the first upwelling pulse by March 22–25.

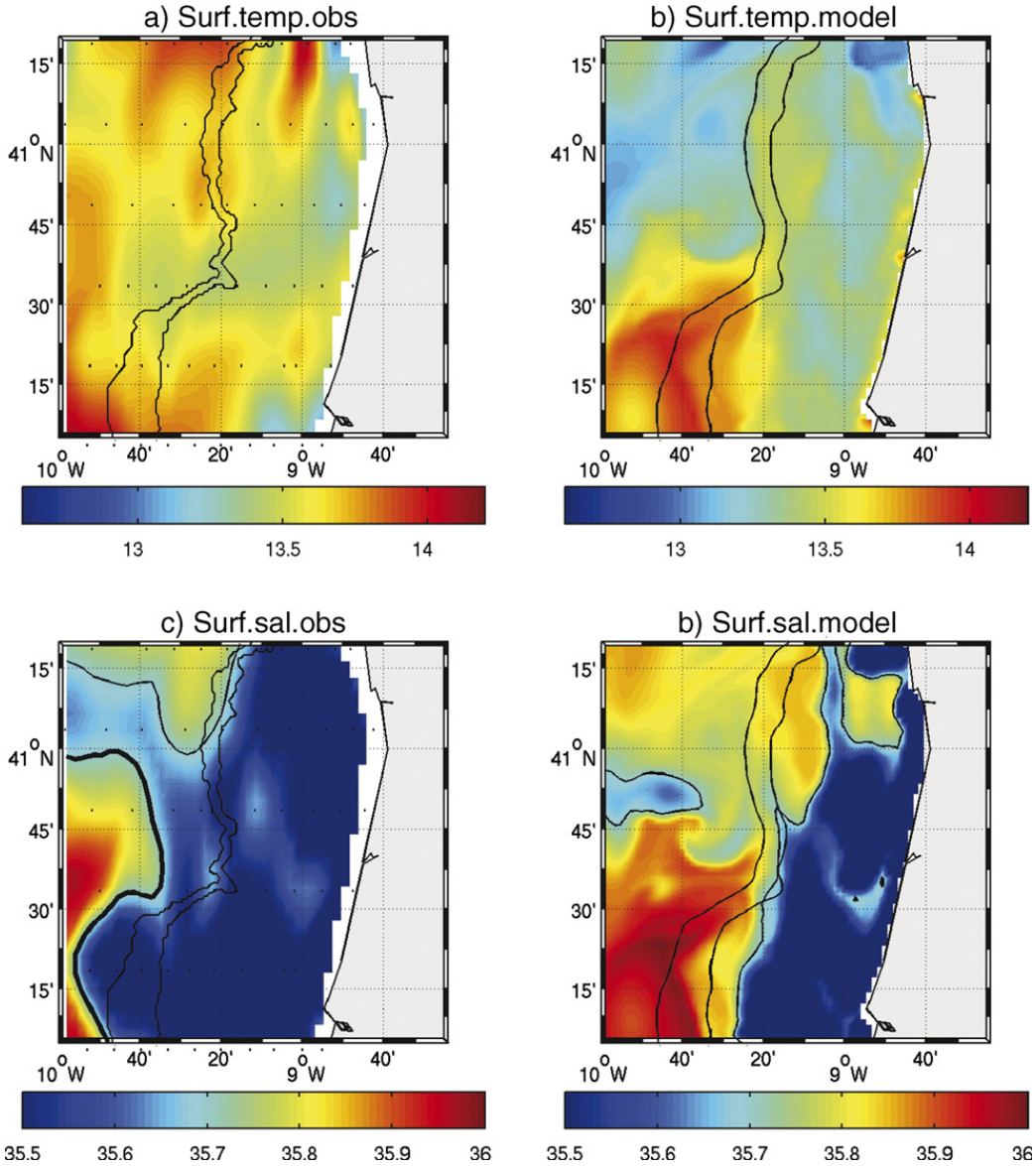

Fig. 4. Surface (10 m) temperature (a) and salinity (c) fields using data from 1991 April survey sections. Model results: b) surface temperature, and d) surface salinity. 200 and 1000 m isobaths are represented. The thick black line corresponds to the 35.7 salinity value. The model time is April 5 1991 which corresponds approximately to the central time of the survey.

The salinity structure clearly dominates the density stratification over the shelf and is represented in Fig. 5 for the CTD (a) and for the model (b). The thick line corresponds to the 35.9 isohaline evidencing the front between the saltier water (dashed values >35.9) of the IPC flowing along the slope and the shelf fresher waters of the WIBP usually under 35.8. In the observed section (Fig. 5a), the core of the IPC (values above 35.95) seems to be shallower (~50 m) than in the model results (Fig. 5a). The core is also displaced offshore (around 9.8°W) when compared with the modeled IPC which is mainly trapped at the slope (9.4°W). On the other hand, the stratification of the real IPC seems larger than in the model slope current (almost homogeneous salinity down to about 250 m). Surface low salinity waters (WIBP) penetrate to about 50 m and show a 30–40 m deep mixed layer. In the case of the observations (a) the extension of the lower salinity waters offshore is more significant (a patch of values below 35.7 is observed offshore west of 9.4°W) than in the model plume. However, the structure is similar in both cases. The offshore progression and mixing of the model plume is a response to the upwelling pulse at the end of March.

The differences between the observed and model plume evolution are in great part associated with the plume–eddy interaction occurring in this zone (see Fig. 4). In the model section (Fig. 5b), part of the plume has separated from the shelf (around 9.9°W). A similar situation is observed in the northernmost cruise sections, since the plume–eddy interaction event seems to have occurred further north in the observations than in the model (Fig. 4). Also the model plume interacts with an IPC that is closer to the upper slope. In this case, mixing and buoyancy loss takes place closer to the shelf, and the offshore penetration of plume waters is weaker.

Comparative statistics of currentmeter data (from reports and from digitalised values) are shown in Table 1. The 40 m depth observations represent the current evolution in the water column. Fig. 3(b) shows the currentmeter time series. The signature of the two upwelling peaks is clear. However, it is interesting to note that although the meridional wind component is always negative during the currentmeter observation period (see Fig. 3), at times of wind relaxation the current is poleward. Winds from Cape Carvoeiro (not shown) also indicate a permanent northerly regime during this period. This means that the background flow in absence of

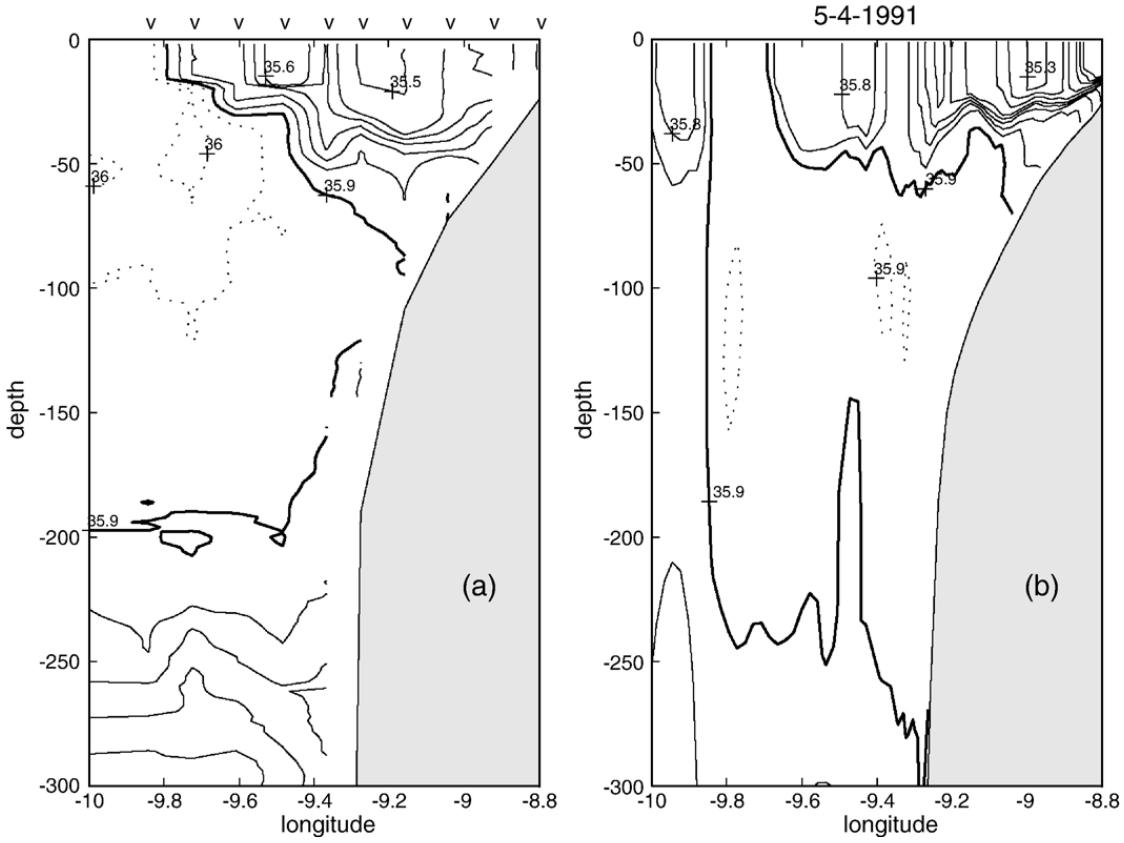

Fig. 5. a) Salinity section from CTD observations (Section IV in Fig. 1), and b) from model results for the same date (April 5) and location. The contour interval is 0.05. The thick line represents the 35.9 salinity value. Dashed lines stand for salinities larger than 35.9.

atmospheric forcing is poleward. This is possibly associated with both the IPC and the cross-shore density front of the WIBP. In response to the first upwelling pulse, the WIBP is advected offshore changing the density-driven currents at midshelf (see Fig. 5).

Model current vectors for the same place and period of mooring deployment are shown in Fig. 3(c) for 37 m model depth. Statistics for the current component time series are presented in Table 1. The observed and model currents time series show a fair agreement, but the model currents are weaker. It is especially noticeable that the second upwelling event (5–8 April) triggers a weak model response when compared with observations. This is probably associated with a larger influence of the slope current in the model results for this period of the simulation and for the zone being represented. Taking into consideration that the initial state is obtained after a spin up with climatology and that the evolution of the IPC is rather turbulent and dependent on the extra coastal density field, the comparison between modeled and observed current values is only qualitative. Nevertheless, the shelf circulation and stratification shows a good match with observed fields.

3.2. Crab larvae distributions and model experiments

3.2.1. Crab larvae distribution in observations

The lack of information about the amount of larvae emission from estuaries and about larvae mortality precludes any quantitative comparison between observed larvae abundances and model floats distributions. In this context, we begin model observations cross-comparisons with a qualitative analysis of dispersion patterns over the shelf. We use the normalised distributions of

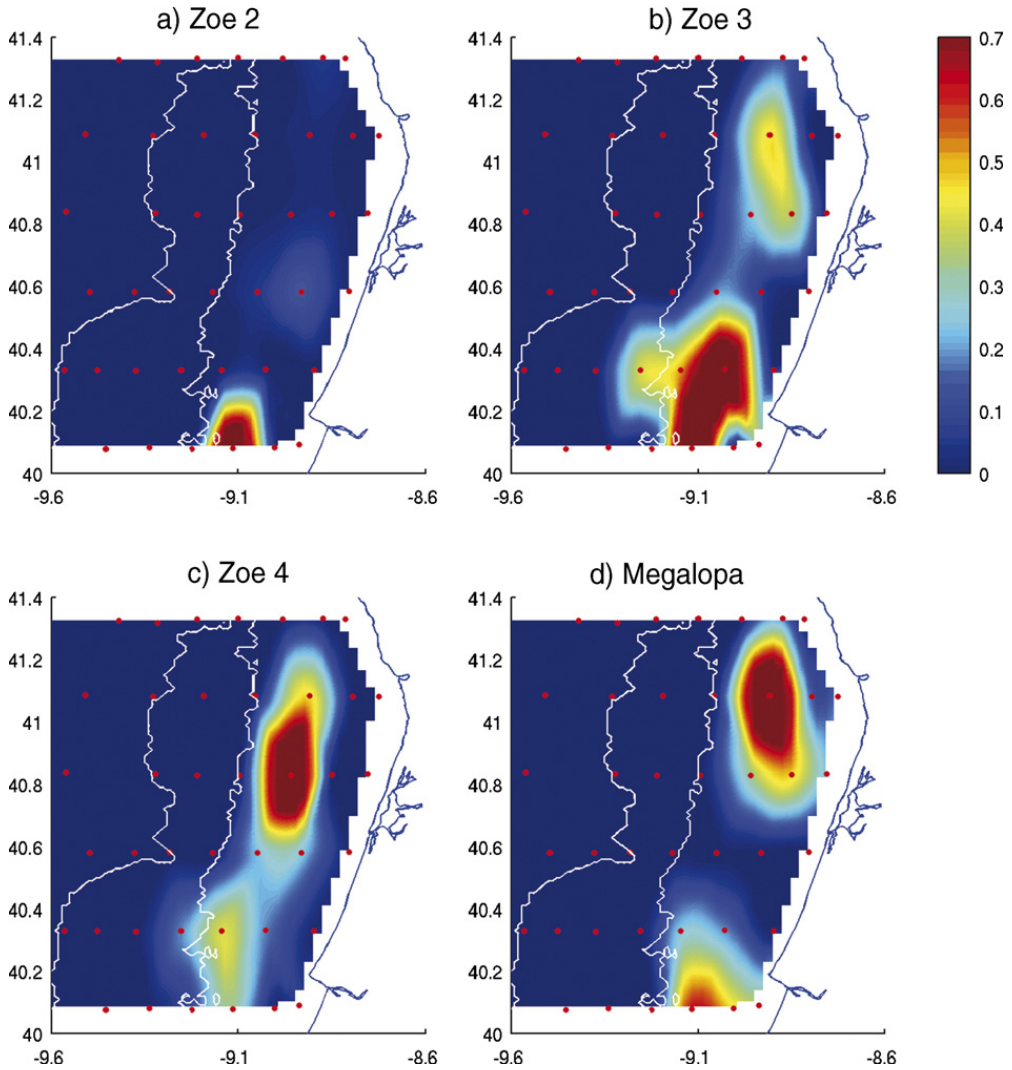

Fig. 6. Maps of normalised larvae concentrations for spring 1991 based on Queiroga (1996). Values above 0.7 are saturated to enhance lower concentration patches. Red dots indicate stations, 200 and 100 m isobaths are represented. a) zoea 2, b) zoea 3, c) zoea 4 and d) megalopa. (For interpretation of the references to colour in this figure legend, the reader is referred to the web version of this article.)

crab larvae for each stage (zoea), and an equivalent quantity for model floats. In the case of observations, we take the concentrations for every station (individuals/m^2 as in Queiroga, 1996) and normalise by the largest concentration recorded (resulting in a value between 0 and 1 for each station and for each zoea). Fig. 6 shows the maps of interpolated normalised larvae concentrations. Red dots indicate the location of the sampling stations. Since the distributions are strongly skewed the values above 0.7 are colour saturated to enhance low concentration patches. Larger patches do not correspond to a larger number of individuals but to a larger number of stations with values close to the maximum value observed (higher level of dispersion).

Map for zoea 1 is not shown since the only significant concentration value was found in the station near Ria de Aveiro (see Fig. 1). This is most probably due to a hatching event during the cruise period (see Table 4). The large majority of larvae is distributed inshore of the 100 m isobath. The larvae are observed within two main patches: One near the southern border, and the second one aligned meridionally along the northern half of the survey area. Zoea 2 (Fig. 6a) is largely concentrated in a station of the southern section 20 to 30 km off the coast. Zoe 2 larvae were probably released to the shelf around March 24 (see Table 4) during the strongest upwelling pulse (Fig. 3a). This possibly explains such strong concentrations in the southern part of the observed area.

3.2.2. Float distributions

A "virtual cruise" was conducted through the model solution to obtain distributions comparable with observations. For each station, the number of floats within a

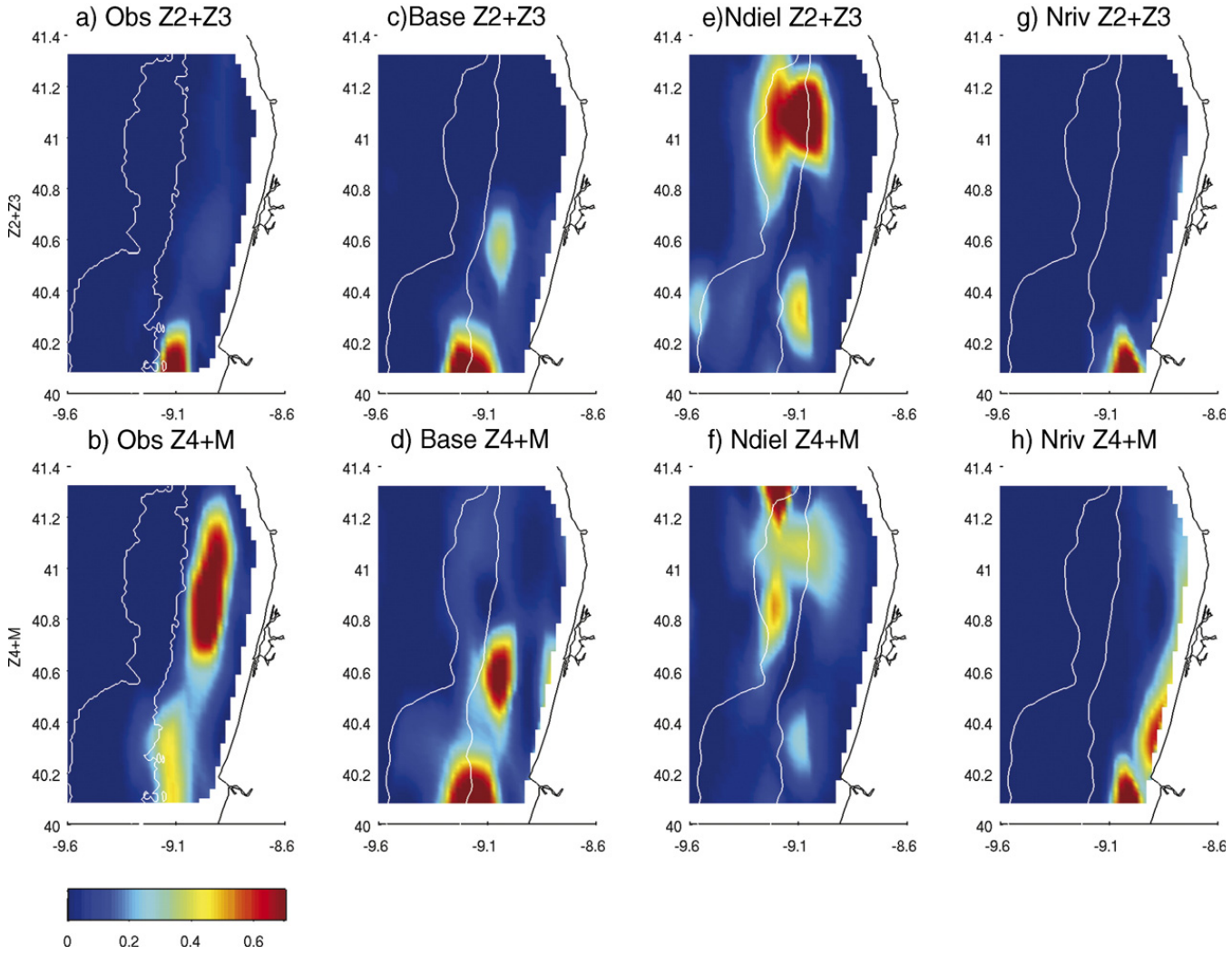

Fig. 7. Maps of normalised concentrations for grouped larvae. Zoeae 2 and 3 upper row and zoea 4 and megalopa lower row. a and b) observations, c and d) Base experiment (Base), e and f) experiment with no diel migration (Nd), and g and h) experiment with no river outflow (Nriv). Values above 0.7 are saturated to enhance low concentration patches. White lines represent 200 and 100 m isobaths. Note that a) and b) look different from a "visual" sum of Fig. 6 panels because of the normalisation.

neighbourhood of less than 4 km (at the time of the station survey) was calculated. Taking into consideration the time since float release (float age) we separate float abundances for each zoea. Afterward, the values were normalised and the maps were reproduced using the same methods as was done for the observations.

Fig. 7 shows distributions for the observations and different model experiments. For the sake of conciseness in the presentation of results, we have grouped larval stages (summed the abundances in each station before normalisation): zoea 2 with zoea 3 (upper row) and zoea 4 with megalopae (lower row). Zoea 1 distributions (not shown) are very similar in the observations and the model since the time lag between the probable date of larvae emission to the shelf and the actual time of float release is rather short (see Table 4).

The model Base experiment (Fig. 7c and d) reproduces the main characteristics of the observed distributions. Almost all floats were found less than 40 km form the coast, with maximum density about 20 km off the shore. Floats generate meridionally elongated patches, and in most stages two cores of float aggregation are observed. The most striking differences concern the northern distribution where model floats are in low concentration (for zoea 4+megalopa). The case with no diel migration (Fig. 7e and f) produces distributions very different from the observations and from the Base experiment. There is a large concentration of floats over the outer shelf and floats aggregate in multiple patches, revealing a pattern of dispersion. For experiments with no river runoff (Fig. 7g and h) the distribution maps are closer to the observations and to the Base experiment but floats tend to drift too close to the coast. A very significant amount of larvae were retained in inshore stations.

In the experiment with varying $\max_d$ (Base 2; not shown), float distributions are similar to the Base

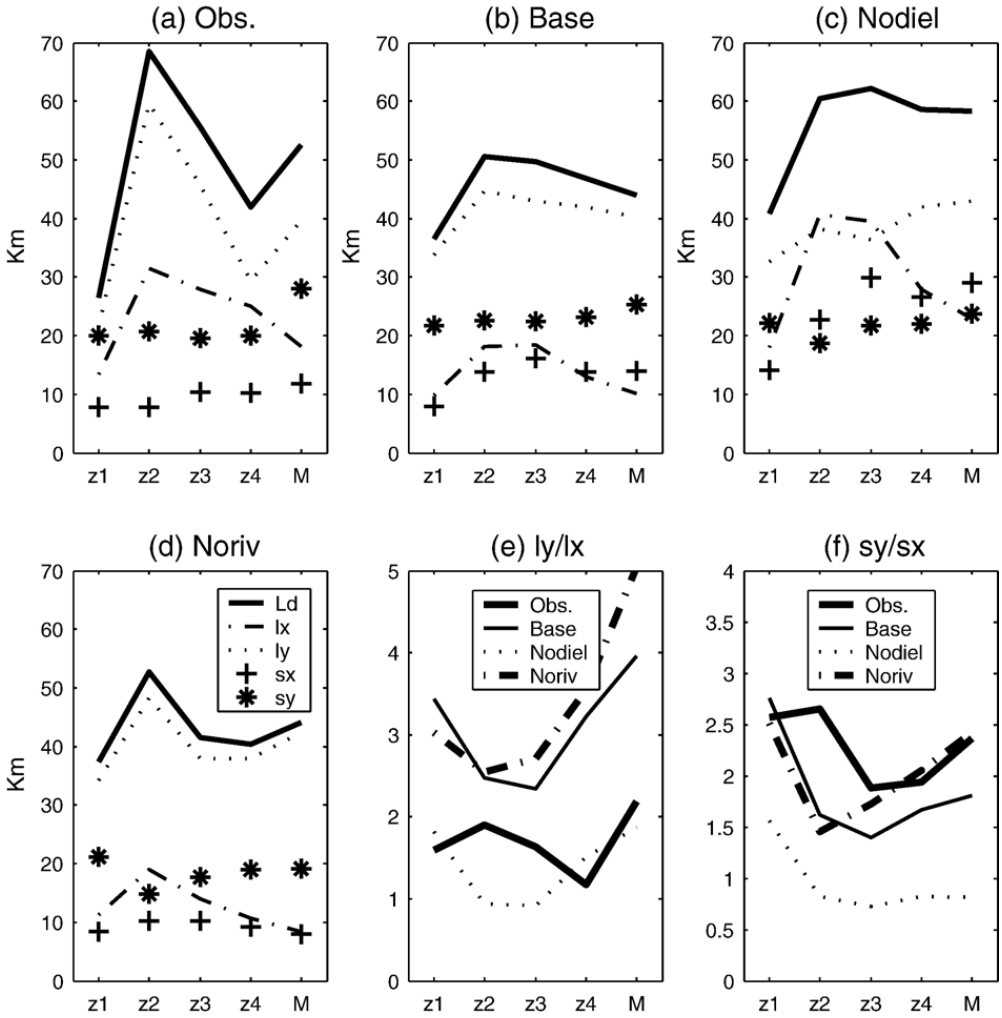

Fig. 8. a) Through d) Dispersal distance (L_d) mean and standard deviations of its meridional and zonal components (l_y, l_x, s_y, s_x) for observations and different model experiments (meaning of each curve is indicated in a legend in d). e) Ratio of meridional to zonal component of dispersion length eccentricity (l_y/l_x) for observations and different model experiments, f) eccentricity calculated with dispersal length variances s_y/s_x. Values are given for all stages (Z1–M).

experiment but with larger dispersion. An opposite effect is obtained in experiments (not shown) with no horizontal diffusion (Nh) or with no vertical diffusion (Nv). These experiments have distributions very similar to the Base case (Fig. 7a and b) but with a much reduced level of dispersion. It is also noteworthy that Nh and Nv are very analogous to each other.

3.3. Dispersal distance

Fig. 8(a–d) show the dispersal distance L_d; its meridional and zonal components (l_y, l_x); and the respective standard deviations (s_y, s_x) for the different zoeae calculated using observations and float experiments. Fig. 8(e and f) show the ratios l_y/l_x and s_y/s_x which will be called here eccentricity for convenience. For the model experiments, statistics are produced using only floats within the limits of the survey area (see Section 2.6 for the methods).

In the observations (Fig. 8a), a considerable variation in L_d is associated with zoea 2 which is possibly too large compared with other zoeae. For the remaining zoeae, L_d is around 40–50 km. The dispersion length is strongly dependent on the meridional component (l_y). The standard deviation of the alongshore component s_y is larger (~20 km) than the zonal (s_x ~ 10 km). Standard deviations increase for older zoeae. The ratios of dispersion characteristics (eccentricity) is shown in Fig. 8e and f (thick line). The meridional dispersion l_y, is about 1.5 to 2 times the zonal value l_x. s_y/s_x is from 2 to 2.5 (Fig. 8f). A significant change of eccentricity with age (zoeae) is not observed.

In the case of the model Base experiment, (Fig. 8b), the mean value for L_d is approximately the same (40 to 50 km) as in the observations. However, the peak in zoea 2 is much lower. l_x, is smaller than in the observations as a significant amount of model floats is retained inshore of the inshoremost stations. However l_y, values are approximately the same as in observations (compare Fig. 8a and b). In what concerns dispersion length standard deviation, the values are very similar to the observed ones. The dispersal length eccentricity l_y/l_x (Fig. 8e) is larger in the model than in the observations. On the other hand, s_y/s_x (Fig. 8f) is smaller in the model results indicating a larger cross-shore patch dispersion.

The float dispersion statistics for the no diel migration experiment (Fig. 8c) are considerably different from the previous case. The meridional component contribution to L_d is very low when compared with observations (Fig. 8a) or with the Base case (Fig. 8b). The zonal dispersion length variance (s_x) is almost always larger than the meridional one s_y (dotted line in Fig. 8f). This indicates that in absence of migration cross-shelf dispersion is higher. A somewhat opposite situation is obtained in the no river runoff experiment (Fig 8d). For this experiment, the contribution of l_x, to the dispersion length is very low (note also that length eccentricity l_y/l_x is the largest among the experiments and observations; Fig. 8e). This is associated with the float retention near the coast when river plumes are weak (see also distributions in Fig. 7g and h).

Suppressing one of the horizontal (Nh) or vertical (Nv) diffusion from the Lagrangian model (not shown) does not change substantially the statistics of dispersion indicating the prevalence of the scales resolved by the ocean model in the Lagrangian transport. These experiments also indicate that explicit horizontal and vertical Lagrangian diffusion have a similar effect on the net dispersion, as has been observed in the sensitivity experiments (see Section 2.3).

3.4. Estimation of real L_d

So far, for the sake of comparison with observations, the statistics of L_d were obtained with float data within the limits of the survey area (regardless of the float release site). Hereinafter, we will use all floats (including those drifting beyond the limits of the survey area) that were

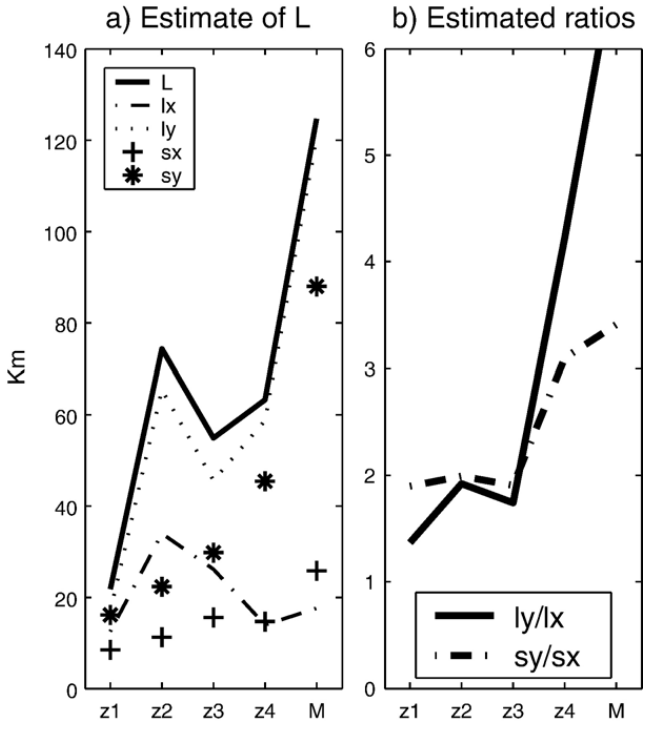

Fig. 9. Dispersal distance L_d and corresponding ratios l_y/l_x and s_y/s_x for the Base experiment with all data (not limited to the observations area), but only using floats released at Ria de Aveiro.

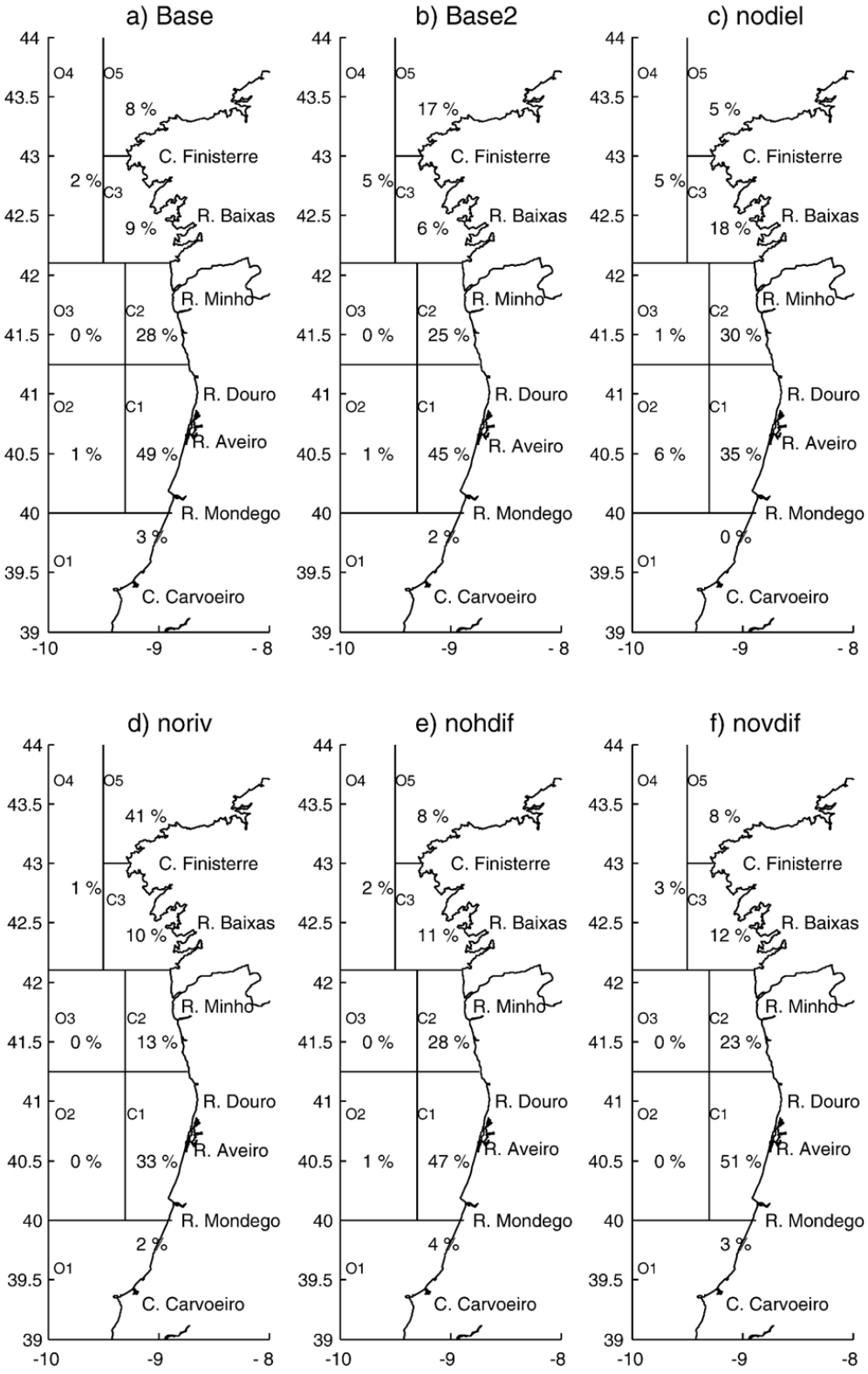

Fig. 10. Percent distributions of floats (corresponding to megalopa stage) for selected areas on April 6. The percent values correspond to the number of floats for a given box divided by the total number of floats in the domain (times 100%).

released at Ria de Aveiro site. The objective is to estimate a real dispersion length L_d for a given emission point.

Fig. 9 shows L_d statistics (a) and eccentricity (b) for the Base case. L_d increases with increasing zoea with the exception of zoea 2 data which above the values for zoeae 3 and 4. For intermediate zoeae L_d is around 50–60 km, and in excess of 120 km for megalopa. This increase is a consequence of the meridional dispersion

since l_x, doesn't change much with float age. Both components of dispersion length variance (s_x and s_y) grow steadily. s_y reaches very large values for megalopa. The eccentricity (Fig. 9b) shows that the meridional component of dispersion becomes increasingly important with time for both the dispersion length and its variance. The values obtained for zoea 2 are very similar to the ones calculated using the observations (compare with Fig. 8a). These high values of L_d for zoea 2 are associated with the response of the floats to the upwelling pulse by 24 of March (Fig. 3). The large increase of L_d for megalopa (>80 km) is possibly not observed in nature. This very high estimates are associated with the fact that the Lagrangian model does not account for mortality and all floats emitted during the first two emission periods (Table 4) reach the megalopa stage (floats about 2 months old exist in the model which is unlikely in nature). In this context, the L_d values for megalopa are possibly overestimated. In summary, these results suggest an estimate for L_d of about 60 km.

3.5. Transport

To evaluate the net Lagrangian transport and potential for settlement along different coastal areas, we have calculated a percent distribution of larvae in selected boxes using all floats at megalopa stage. Fig. 10 presents the results for 6 different experiments. Percentages in each box indicate the presence of megalopae within the box relative to the total amount of megalopae counted in the experiment on April 6. The boxes are constructed to include representative coastal (C) and oceanic (O) areas. In the coastal zone, we define Cl: the main estuaries used to release the floats; C2: a group of northern estuaries between Rivers Douro and Minho; and C3: the coastal system of Rias baixas. The oceanic boxes were selected to estimate the transport of larvae to the south (01), to the north (05) and to the deep ocean (02, 03, and 04).

With the exception of the no river runoff experiment, all cases show a high degree of float retention (~50%) in the central box (Cl). The largest part of remaining megalopae were transported northward and a very small number of floats were lost to the south (<4%). In all cases, the offshore transport was small, and the most significant values correspond to the no diel migration case (6%; 02 in Fig. 10c). It is found that estuaries north of Douro (boxes C2 and C3) are potential recruitment zones in all conditions. The recruitment potential to the south of Mondego River is minimal. Base 2 experiment (Fig. 10b) is very similar to the Base experiment, showing that varying the maximum depth of DVM is not a critical factor for the net transport. The no diel migration case (Fig. 10c) is as expected the one with the most significant differences. A substantial reduction (~15%) of retention near the float release points is noticed. Float export to the deep ocean is found along different shelf sites. The experiment with no river runoff (Fig. 10d) shows the largest transport of floats to the

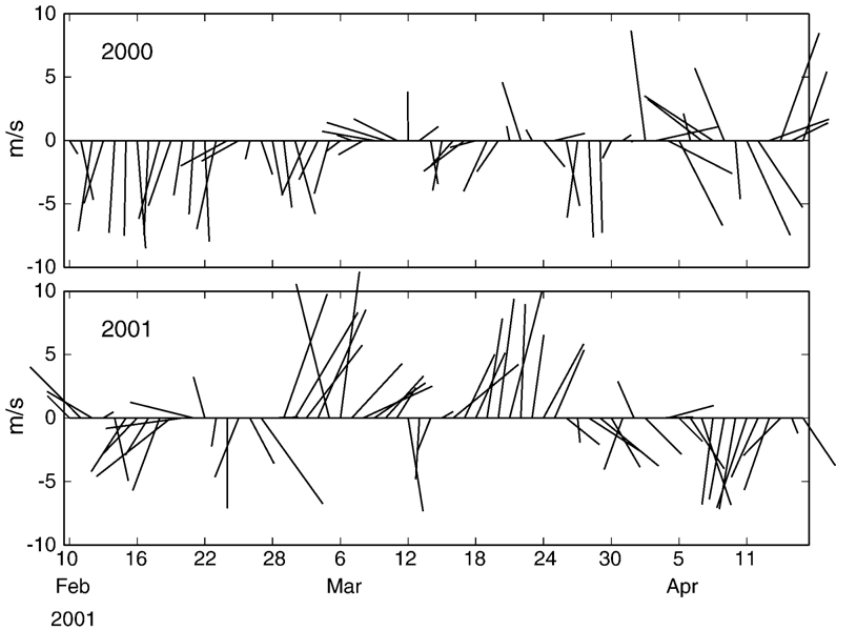

Fig. 11. Wind stick plots for 2000 and 2001 from the same location and same year dates as 1991 series (Fig. 3).

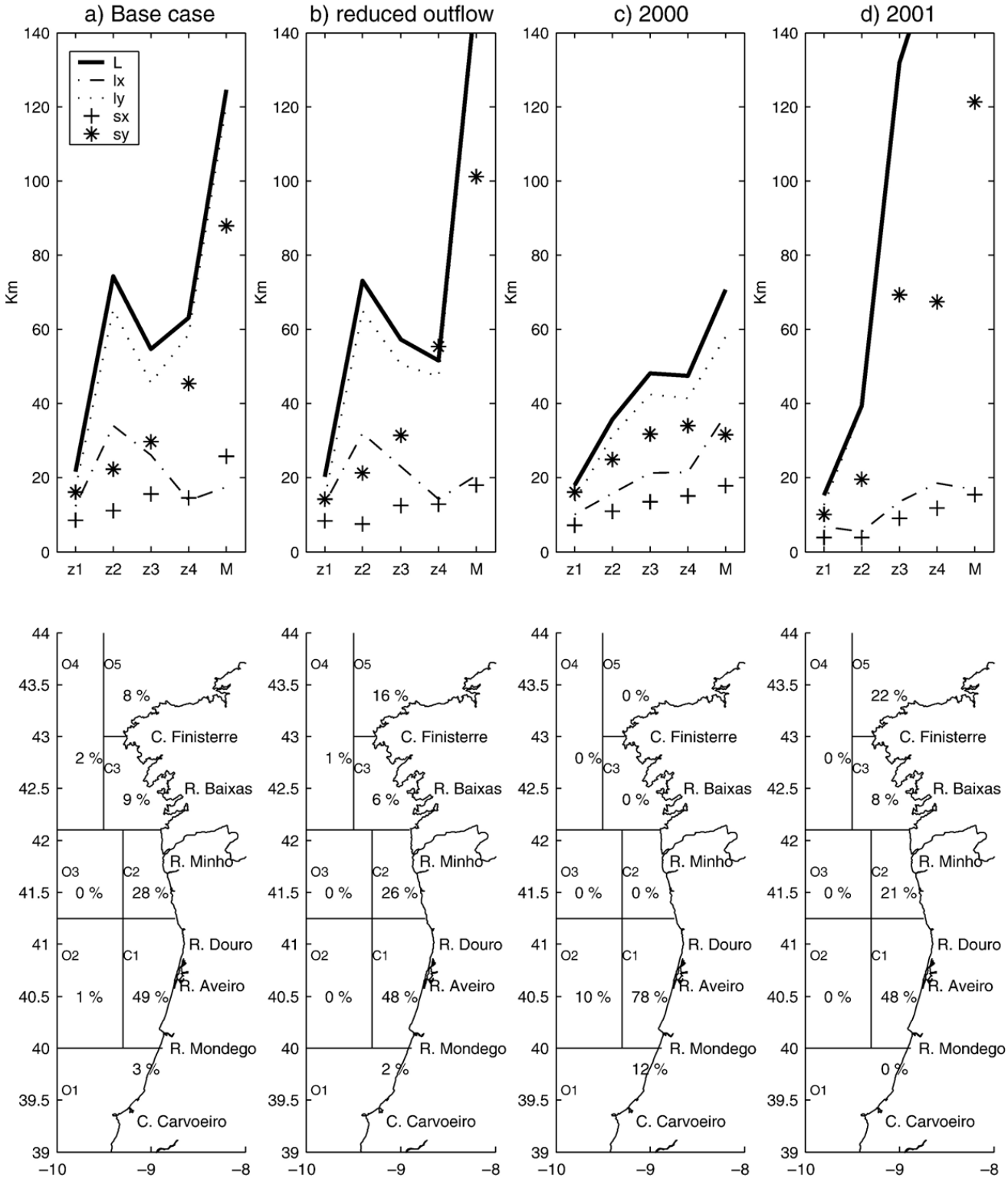

Fig. 12. Top row shows L_d statistics (same as Fig. 9) and bottom row shows percent distributions (same as Fig. 10) for experiments with varying oceanographic conditions. a) and b) Base case replicated from Fig. 9 and Fig. 10 for convenience; b) reduced outflow; c) atmospheric forcing from 2000; d) atmospheric forcing from 2001.

north of the emission area (41% in O5). In this experiment, the maximum northward floats displacement (not shown) is around 400 km while the southernmost detected float is less than 200 km from the emission area. Experiments with no explicit Lagrangian diffusion in the horizontal (Fig. 10e) or in the vertical (Fig. 10f) do

not show significant differences when compared with the Base case.

In summary, nearly half of the floats (at megalopa stage) are retained near the emission point (Cl). The net Lagrangian transport is very sensitive to DVM (experiments with no diel migration show a much reduced level of retention in the central box (C1) but not very responsive to the details of vertical migration (no significant differences between Base and Base 2). Finally, the experiments show that the transport patterns change significantly with river plume activity. Low river runoff contributes to inshore retention and to larger northward transport.

3.6. Varying oceanographic conditions

So far all Lagrangian experiments were conducted using the atmospheric forcing conditions for 1991 (validated with observations). Additional experiments with atmospheric forcing from other years and different river runoff values were done to study the sensitivity of dispersion patterns to varying oceanographic conditions. Fig. 11 shows wind vectors for the period February–April of years 2000 and 2001, to be compared with wind vectors of year 1991 for the same season and spatial location (Fig. 3). These two years were selected because they have a significantly different mean meridional wind component ($\overline{v}$). For the February–April period of 1991 $\overline{v}=-1.66$ m/s. During the same period of 2000, the upwelling-favourable events dominated and $\overline{v}=-2.11$ m/s. The opposite situation is registered during February–April of 2001 when downwelling superseded upwelling and the meridional wind component $\overline{v}=0.15$ m/s. With the exception of the atmospheric forcing all other conditions in the model were equal to the 1991 case (Base case). Additionally, in order to test the Langrangian transport sensitivity to river runoff conditions, an experiment with reduced river outflow (1/4 of the values used in the Base experiment) was conducted with the atmospheric forcing conditions of 1991.

Fig. 12 shows the L_d statistics (equivalent to Fig. 9a) and megalopae transport budget calculations (equivalent to Fig. 10). The dispersion statistics in the case of reduced outflow (Fig. 12b), do not show significant differences from the Base case (Figs. 12a), although the float concentration in the northernmost box (O5) is doubled. This confirms the role of weak plumes in reducing the offshore transport and in increasing the export of floats to the northern coastal areas. However, the difference from the complete absence of river plumes case is still considerable (see results for the no river runoff experiments in Fig. 10d).

The experiment with the atmospheric forcing of year 2000 (Fig. 12c), is significantly different from the Base case (Fig. 12a). The L_d statistics reveal a much reduced l_y, and a larger l_x, (lower eccentricity) for older zoeae. The float budgets (Fig. 12c lower row) present a very small meridional transport though winds were upwelling-favourable most of the time (see Fig. 11). 0% concentration in all the northern boxes and only 12% were transported to the south (box O1). However, a striking value of retention (78%) is found over the shelf area C1 where the floats were released. Finally, the offshore transport (10%) is as important as the southward transport and has the largest value among all experiments (see also Fig. 10).

The experiment with 2001 atmospheric forcing (Fig. 12d) shows an extreme meridional dispersion associated with a very large northward transport resulting in the largest concentration of megalopae in the northern box (O5) apart from the experiment with no river runoff (Fig. 10d). All offshore and southern boxes have null values but the retention in the central box (C1) is of the same order as in the Base experiment. The values for l_x, (Fig. 12d) are very low (10–20 km) indicating that the floats are retained very close to the coast.

In summary, the experiments show that the dispersal patterns are very sensitive to the wind, but an asymmetrical response is observed. In the case of significant upwelling activity (2000) the net southward Lagrangian transport is increased (12% of floats south of C1) but this change is much less dramatic than the increase in northward transport driven by dominant downwelling favourable winds (52% of floats north of C1 in the 2001 forcing case). Nonetheless, the mean wind in absolute values was stronger for the upwelling case $\overline{v}=-2.11$ m/s than for the downwelling case $\overline{v}=0.15$ m/s. The net Lagrangian transport is therefore preferentially northward. In addition, weaker river plume activity contributes to an increase of this northward transport.

4. Discussion

4.1. Along-shore distribution

Floats tend to aggregate along band-like meridional patches parallel to the coast usually inshore of the 100 m. This aggregation is often observed in nature (e.g., Queiroga, 1996). Our numerical experiments indicate that this dispersal pattern is associated with the vertical migratory movement that forces floats to disperse with the vertically integrated flow which is mainly alongshore. A second factor contributing to this meridional distribution is the alternating nature of the

along-coast winds during the spring transition period off Western Iberia.

The shelf flow is weakly stratified and the wind-driven circulation is essentially barotropic and intensified at the near shore zones. Downwelling events push the floats into the core of the wind-driven poleward jet. Near the coast, the floats rapidly progress along-shore and the patches elongate. During upwelling, the floats move offshore, away from the core of the equatorward current reducing their southward transport. The intermittency of downwelling and upwelling events contributes to the meridional dispersal of larvae and to a preferentially net northward Lagrangian transport.

4.2. River plumes and layer Ekman dynamics

The case of no river runoff is contrary to expectations. River plumes can act as transport conduits (e.g., Garvine et al., 1997) once they generate advecting currents with the coast on its right. In the case of important river runoff larger northward transport is expected. However, our results show the opposite for the floats net transport. Experiments with river plumes show reduced northward net Lagrangian transport.

The apparent contradiction is caused by the interplay between buoyancy input from river plumes and Ekman layer dynamics. River runoff plumes are able to affect surface stratification, and consequently the Ekman layer dynamics. In the case of weak or inexistent buoyancy input from river plumes, surface stratification decreases, the Ekman layer thickens and the cross-shore extension of the innershelf (where surface and bottom Ekman layers merge) increases. The innershelf has modified Ekman dynamics with reduced cross-shelf flow and increased along-shore (along-wind) currents which favours along-shore Lagrangian transport in the wind direction. Downwelling events should favour further mixing and enlargement of the innershelf zone (see Austin and Barth, 2003). On the contrary, upwelling events may contribute to water column restratification through density input from the bottom (e.g., Austin and Lentz, 2002), although that may only be true in the first stage of an upwelling event (see a detailed study in Estrade, 2006). Innershelf dynamics combined with river runoff stratification effect may therefore contribute to the asymmetry in meridional transport between upwelling and downwelling cases.

4.3. Unresolved physics

The good statistical comparison between model and observations indicates that the major physical processes driving larvae dispersion were well represented at the scales considered. Inclusion of explicit diffusion in the Lagrangian model further improves the comparison between model and observations of L_d statistic. However, it is interesting to note that no significant differences were found between the effects of horizontal and vertical diffusion. This is possibly associated with the fact that in flows with a significant vertical shear the vertical diffusion may play a role similar to the horizontal diffusion (e.g., Largier, 2003). Other aspect still missing from the model physics is the change of horizontal diffusion at the coastal lateral boundary layer (e.g., Largier, 2003). In this zone, the cross-shore diffusion is much smaller and coastal retention is enhanced further modifying the retention processes in the innershelf zone. This process should be accounted for in future modelling studies.

4.4. Vertical migration

A thoroughly study of all aspects of vertical migration (DVM) was not conducted because of the lack of knowledge about the details of this diurnal behaviour (see Queiroga and Blanton, 2005, for a review). A study of the effects of migrations on the retention of crab larvae is presented in Marta-Almeida et al. (2006). The authors conclude that diel migration is a very important factor for the retention of floats inshore, but the different schemes of DVM that were tested did not lead to significantly different results. Our no DVM experiment shows important differences from the Base case (with DVM). However, the floats net transport is not very sensitive to the details of the vertical migration scheme since (Base and Base 2 cases show similar transport statistics). For this reason, the results of this study can be extrapolated to other invertebrate larvae with DVM (e.g., Queiroga and Blanton, 2005).

4.5. Dispersal length L_d

We estimate $L_d \sim 60$ km for the intermediate zoeae but a much larger value for megalopae (over 100 km). However, this value is possibly overestimated due to the fact that mortality is not included in the Lagrangian model. Shanks et al. (2003) gather some values of L_d found in literature; A wide range of rather high values (161–173 km) were calculated for the west coast of North America while a smaller value (63 km) is given for the east coast. According to the authors, the difference in dispersal length estimates is associated with different speed regimes of coastal currents. The west

coast of North America is characterised by strong coastal upwelling jets and counter flows whereas the east coast shelf currents are lower in magnitude. Western Iberia during the spring-transition (the study period) is closer in currents magnitude to the east coast of North America. The winds are intermittent and no strong upwelling events are observed. In this context, our value of 60 km matches the estimate for the east coast of North America.

4.6. Impact on population dynamics

The importance of dispersal distances to the local population dynamics is discussed in Largier (2003). Using a simple model setup this author shows that both advective and diffusive processes of dispersion should be considered in dispersal estimates. If L and S represent the dispersal distances associated with advective and diffusive effects, respectively, then, for a given population, if $L \gg S$ this population will be a source of larvae for other populations and unlikely a point of recruitment for its own larvae. This type of system is characterised as advective. If, in the opposite case $L \ll S$, the system is diffusive and the population recruits its own larvae. Finally, the difference $L - S$ is also important. For two populations to comunicate it is important that the distance between them is larger than $L - S$ but smaller than $L + S$.

In our float results, there is no explicit separation between advective and diffusive effects. However, since the float path is an integration of advection and diffusion we can approximately take our estimates of mean dispersal length (l) as the advective effect, and its standard deviation (s) as the diffusive components of dispersion. According to our estimates above (Section 3.4) $l \sim 60$ km and $s \sim 20$ km, meaning that communicating populations should be between 40 and 80 km apart. It is interesting to notice that the distances between estuaries are within this range (see Fig. 1).

In view of the present results, we can draw some speculations regarding population dynamics of Western Iberia. The estuaries that were used as emission points in the model (River Mondego, Ria de Aveiro, and River Douro; Fig. 1) are communicating populations and export larvae to the northern estuaries up to Minho River. If these estuaries are also sources of larvae, these populations may be linked up to Finisterre (Fig. 1). North of this point, the retention conditions imposed by winds and coast line orientation change in a significant way, so that L_d and the retention processes discussed above are most probably different. To the south of the main emission points (south of River Mondego; Fig. 1), the transport is very small. Moreover, the distance to the major southern estuary of (River Tagus) is above the critical value ($l_y + s_y \approx 80$ km) for populations to communicate.

5. Summary and conclusion

A dispersal study was conducted for the Western Iberian shelf using a nested general circulation model with a Lagrangian submodel. The results show good comparison with observations. The floats mainly disperse along patches parallel to the coast usually inshore of 100 m isobath. This pattern is strongly controlled by the local wind-driven circulation, the coastline orientation, and the ability of larvae to diurnally move up and down in the water column (die1 vertical migration). A large number of floats ($\sim 50\%$) are retained in the vicinity of the emission zone even after periods of significant wind events (especially upwelling). River plumes are critical factors in the retention patterns through the buoyancy input and stratification near the coast influencing the cross-shore and along-coast transport. In the case of no river input, floats are largely retained at the innershelf and the transport occurs near the coast downwind. The net northward transport during downwelling events is larger than the net southward transport during upwelling episodes of similar magnitude. In case of alternating wind episodes, the net transport is preferentially northward. Coupling between atmospheric conditions and river runoff may modulate the interannual variability and introduce significant changes in the plankton transport. Dispersion distances (L_d) of about 60 km ($s \sim 20$ km) were estimated essentially representative of the meridional component of dispersion. From the point of view of population dynamics it is suggested that the estuaries of the Northwest Iberia are communicating populations sharing similar conditions of dispersion and retention: coastline orientation, alternating winds during late winter and spring, river plumes and distance between communicating estuaries. These conditions are changed north of Cape Finisterre and to south of Cape Carvoeiro.

Acknowledgements

This publication is the corollary of a collaborative project between the University of Aveiro, and the Institute of Research for Development under the Portugal–France integrated actions (Pessoa-Egide) and the FCT project (ProRecruit-POCTI/BSE/36663/99). Financial support was allocated by FCT under the Support Community

Framework III, Operational Programme Science, Technology and Innovation. Alvaro Peliz was partially funded by the Fundação para a Ciência e a Tecnologia through the CESAM pluriannual programme, and in the frame of the FCT Post-Doc programme contract (BPD/16777/2004). The authors gratefully acknowledge all participants in the WOCE II April observation programme off Western Iberia, and to the NCEP/NCAR reanalysis project of the NOAA-CIRES Climate Diagnostics Center. The authors wish to thank the anonymous reviewers for their very important comments and suggestions.

References

Álvarez-Salgado, X.A., Figueiras, F.G., Pérez, F.F., Groom, S., Nogueira, E., Borges, A.V., Chou, L., Castro, G.C., Moncoiffé, G., Rios, A.F., Miller, A.E.J., Frankignoulle, M., Savidge, G., Wollast, R., 2003. The Portugal Coastal counter current off NW Spain: new insights on its biogeochemical variability. Progress in Oceanography 56, 281–321.

Austin, J., Barth, J., 2003. Drifter behaviour on the Oregon-Washington Shelf during downwelling favourable winds. Journal of Physical Oceanography 32, 3132–3144.

Austin, J., Lentz, S., 2002. The inner shelf response to wind-driven upwelling and downwelling. Journal of Physical Oceanography 32, 2171–2193.

Capet, X.J., Marchesiello, P., McWilliams, J.C., 2004. Upwelling response to coastal wind profiles. Geophysical Research Letters 13, L13311. doi:10.1029/2004GL020123.

da Silva, A.M., Young, C.C., Levitus, S., 1994. Atlas of Surface Marine Data 1994 — NOAA Atlas NEDIS.

Dawirs, R.R., 1985. Temperature and larval development of *Carcinus maenas* (Decapoda) in the laboratory; prediction of larval dynamics in the sea. Marine Ecology. Progress Series 24, 297–302.

Estrade, P., 2006. Mecanism of upwelling separation from the coast on wide and shallow shelves off Northwest Africa. PhD thesis. University of Western Britanny, France.

Garvine, R.W., Epifanio, C.E., Epifanio, C.C., Wong, K.C., 1997. Transport and recruitment of blue crab larvae: a model with advection and mortality. Estuarine, Coastal And Shelf Science 45, 99–111.

Hagen, 1994. Berichte des Bundessamtes fur Seeschiffahrt und Hidrographie, vol. 2. Hamburg-Rostock.

Haidvogel, D.B., Beckman, A., 1999. Numerical Ocean Circulation Modeling. Imperial College Press.

Haynes, R., Barton, E.D., Pilling, I., 1993. Development, persistence and variability of upwelling filaments off the Atlantic Coast of the Iberian Peninsula. Journal of Geophysical Research 98 (C12), 22681–22692.

Kline, H., 2000. The Subsurface Eastern Boundary Current of the North Atlantic Between 32N and Data Report. Bundesamt fur Seeschiffahrt und Hydrographie.

Large, W.G., McWilliams, J.C., Doney, S.C., 1994. Oceanic vertical mixing: a review and a model with a nonlocal boundary layer parameterization. Reviews of Geophysics 32, 363–403.

Largier, J.L., 2003. Considerations in estimating larval dispersal distances from oceanographic data. Ecological Applications 13 (1), S71–S89.

Levitus, S., Boyer, T.P., Antonov, J., Burgett, R., 1994a. World Ocean Atlas 1994 Volume 4: Temperature —NOAA Atlas NESDIS.

Levitus, S., Burgett, R., Boyer, T.P., 1994b. World Ocean Atlas 1994 Volume 4: Salinity — NOAA Atlas NESDIS.

Marchesiello, P., McWilliams, J.C., Shchepetkin, A., 2001. Open boundary conditions for long-term integration of regional oceanic models. Ocean Modelling 3, 1–20.

Marchesiello, P., McWilliams, J.C., Shchepetkin, A., 2003. Equilibrium structure and dynamics of the California Current System. Journal of Physical Oceanography 33, 753–783.

Marta-Almeida, M., Dubert, J., 2006. The structure of tides in the Western Iberia Region. Continental Shelf Research 26, 385–400.

Marta-Almeida, M., Dubert, J., Peliz, A., Queiroga, H., 2006. Influence of vertical migration pattern on retention of crab larvae in the shelf in a seasonal upwelling system. Marine Ecology Progress Series 307, 1–19.

Monin, A.S., Ozmidov, R.V., 1981. Ocean Turbulence. Gidrometeoizdat, Leningrad.

Nagaraj, M., 1993. Combined effects of temperature and salinity on the zoeal development of the green crab, *Carcinus maenas* (Linnaeus, 1758) (Decapoda: Portunidae). Seientia Marina 57, 1–8.

Peliz, A., Rosa, T., Santos, A.M.P., Pissara, J., 2002. Jets, eddies, and counterflows in the Wester Iberia upwelling system. Journal of Marine Systems 35, 61–77.

Peliz, A., Dubert, J., Haidvogel, D.B., Le Cann, B., 2003. Generation and unstable evolution of a density-driven eastern current: the Iberian current. Journal of Geophysical Research 108 (C8), 3268. doi:10.1029/2002JC001443.

Peliz, A., Dubert, J., Santos, A.M.P., Le Cann, B., 2005. Winter upper ocean circulation in the western Iberia Basin. Fronts, eddies and flows: an overview. Deep-Sea Research. Part 1. Oceanographic Research Papers 52, 621–646.

Penven, P., 2003. ROMSTOOLS User's Guide. Tech. Rep.. IRD. http://fraise.univ-brest.fr/penven/roms_tools/.

Penven, P., Debreu, L., Marchesiello, P., McWilliams, J.C., 2006. Evaluation and application of the ROMS l-way embedding procedure to the central California Upwelling System. Ocean Modelling 12, 157–187.

Queiroga, H., 1996. Distribution and drift of the crab *Carcinus maenas* (L.) (Decapoda, Portunidae) larvae over the continental shelf off northern Portugal in April 1991. Journal of Plankton Research 18, 1981–2000.

Queiroga, H., 1998. Vertical migration and selective tidal stream transport in the megalopa of the crab *Carcinus maenas*. Hydrobiologia 375/376, 137–149.

Queiroga, H., Blanton, J.O., 2005. Interactions between behaviour and physical forcing in the control of horizontal transport of decapod crustaceans larvae: an overview. Advances in Marine Biology 47, 107–214.

Queiroga, H., Costlow Jr., J.D., Moreira, M.H., 1994. Larval abundance patterns of *Carcinus maenas* (Decapoda, Braehyura) in Canal de Mira (Ria de Aveiro, Portugal). Marine Ecology. Progress Series 111, 63–72.

Queiroga, H., Costlow Jr., J.D., Moreira, M.H., 1997. Vertical migration of the crab *Carcinus maenas* first zoea in an estuary: implications for tidal stream transport. Marine Ecology. Progress Series 149, 121–132.

Rice, A.L., Ingle, R.W., 1975. The larval development of *Carcinus maenas* (L.) and *C. mediterraneus* Czerniavsky (Crustaeea, Braehyura, Portunidae) reared in the laboratory. Bulletin of the British Museum, Natural History. Zoology 28, 103–120.

Ross, O.N., Sharples, J., 2004. Recipe for 1-D Lagrangian particle tracking models in space varying diffusivity. Limnology and Oceanography 2, 289–302.

Santos, A.M.P., Peliz, A., Dubert, J., Oliveira, P.B., Angelieo, M.M., Re, P., 2004. Impact of a winter upwelling event on the distribution and transport of sardine eggs and larvae off Western Iberia: a retention mechanism. Continental Shelf Research 24, 149–165.

Shanks, A.L., Grantham, B.H., Carr, M.H., 2003. Propagule dispersal distance and the size and spacing of marine reserves. Ecological Applications 31 (1), S159–S169.

Shchepetkin, A., McWilliams, J.C., 2003. A method for computing horizontal pressure-gradient force in an ocean model with a non-aligned vertical coordinate. Journal of Geophysical Research 108 (C3), 3090. doi:10.1029/2001JC001047.

Shchepetkin, A., McWilliams, J.C., 2005. The regional oceanic modeling system: a split-explicit, free-surface, topography-following-coordinate ocean model. Ocean Modelling 9, 347–404.